Molecular Systems Biology (2006) doi:10.1038/msb4100107

www.molecularsystemsbiology.com
Article number: 67

molecular systems biology

A stochastic model of *Escherichia coli* AI-2 quorum signal circuit reveals alternative synthesis pathways

Jun Li[1,2], Liang Wang[1,3], Yoshifumi Hashimoto[1], Chen-Yu Tsao[1,4], Thomas K Wood[5], James J Valdes[6], Evanghelos Zafiriou[4] and William E Bentley[1,2,4,*]

[1] Center for Biosystems Research, University of Maryland Biotechnology Institute, College Park, Maryland, MD, USA, [2] Fischell Department of Bioengineering, University of Maryland, College Park, Maryland, MD, USA, [3] Department of Cell Biology and Molecular Genetics, University of Maryland, College Park, Maryland, MD, USA, [4] Department of Chemical and Biomolecular Engineering, University of Maryland, College Park, Maryland, MD, USA, [5] Department of Chemical Engineering, Texas A&M University, College Station, TX, USA and [6] Edgewood Chemical Biological Center, US Army, Aberdeen Proving Ground, MD, USA
* Corresponding author. Center for Biosystems Research, University of Maryland Biotechnology Institute, 5115 Plant Science Building, College Park, Maryland, MD 20742. USA. Tel.: +1 301 405 4321; Fax: +1 301 314 9075; E-mail: bentley@eng.umd.edu

Received 2.3.06; accepted 18.9.06

Quorum sensing (QS) is an important determinant of bacterial phenotype. Many cell functions are regulated by intricate and multimodal QS signal transduction processes. The LuxS/AI-2 QS system is highly conserved among Eubacteria and AI-2 is reported as a 'universal' signal molecule. To understand the hierarchical organization of AI-2 circuitry, a comprehensive approach incorporating stochastic simulations was developed. We investigated the synthesis, uptake, and regulation of AI-2, developed testable hypotheses, and made several discoveries: (1) the mRNA transcript and protein levels of AI-2 synthases, Pfs and LuxS, do not contribute to the dramatically increased level of AI-2 found when cells are grown in the presence of glucose; (2) a concomitant increase in metabolic flux through this synthesis pathway in the presence of glucose only partially accounts for this difference. We predict that 'high-flux' alternative pathways or additional biological steps are involved in AI-2 synthesis; and (3) experimental results validate this hypothesis. This work demonstrates the utility of linking cell physiology with systems-based stochastic models that can be assembled *de novo* with partial knowledge of biochemical pathways.
Molecular Systems Biology 12 December 2006; doi:10.1038/msb4100107
Subject Categories: metabolic and regulatory networks; microbiology and pathogens
Keywords: AI-2; DPD; LuxS; quorum sensing; stochastic model

Introduction

Bacteria utilize an intricate communication system for sensing and interpretation of environmental cues that has recently been shown to mediate coordinated population-based behavior. This process, termed 'quorum sensing' (QS), involves the production, the release and detection of small chemical signal molecules, called autoinducers. Conceptually, a threshold stimulatory concentration of autoinducer is achieved, then a signal transduction cascade is initiated that ultimately results in a change of the 'collective' behavior of the organism (Nealson *et al*, 1970; Fuqua and Greenberg, 1998; Miller and Bassler, 2001). QS has been found to be a regulator of cellular processes such as bioluminescence production (Bassler *et al*, 1994; Miller and Bassler, 2001), virulence gene expression (Zhu *et al*, 2002), biofilm formation (Balestrino *et al*, 2005; Yoshida *et al*, 2005), cell division, motility, metabolism, and recombinant protein production (DeLisa *et al*, 2001a, b; Sperandio *et al*, 2002). Indeed, QS is an integral component of global gene regulatory networks (Withers *et al*, 2001), and has been suggested to be 'a language for bacteria', mediating social engagements between prokaryotes and eukaryotes (Sperandio *et al*, 2003; Williams *et al*, 2004; Vendeville *et al*, 2005).

There are several types of QS systems, including (1) an acylated homoserine lactone (AI-1) system used by a variety of Gram-negative bacteria (Fuqua *et al*, 2001), (2) a post-translationally modified peptide signaling system of Gram-positive species (Sturme *et al*, 2002), and (3) a system mediated by a highly conserved autoinducer synthase, LuxS, which appears among a variety of Gram-negative and Gram-positive bacterial species (Surette *et al*, 1999; Federle and Bassler, 2003; Sperandio *et al*, 2003; Xavier and Bassler, 2003). Because of its cross-species and even pro–eukaryotic connectivity, the *luxS*-mediated system has been the topic of intense research. The most well-studied *luxS*-derived autoinducer, AI-2, is a product of the activated intracellular methyl cycle, and the flux of metabolites through this cycle affects the rate of its formation (Posnick and Samson, 1999; Winzer *et al*, 2003). Indeed, the production rate of AI-2 has been shown to be linearly proportional to cell growth rate (DeLisa *et al*, 2001a). Alternatively, its level in batch cultures in the extracellular medium appears to be modulated by a sophisticated autoregulated energy-dependent mechanism, suggesting an important cellular function (Xavier and Bassler, 2005). Understanding the intricacies of AI-2-mediated regulation and the mechanisms by which AI-2 influences transcription and/or cellular phenotype will naturally play a role in deciphering

the behaviors of these *luxS*-containing bacteria in various environments.

Large-scale system biology platforms for transcriptomics, proteomics, and metabolomics enable transient experimental mapping of biological systems; however, the conceptual framework of these genetic systems cannot be fully developed without computational or simulation approaches. That is, the mathematical models serve to integrate experimental data as well as facilitate hypotheses that can be tested, and serve to provide valuable insights into the general principles of biological system organization (Westerhoff and Palsson, 2004).

In this work, a stochastic model based on the algorithms of Gillespie (1977) was used to simulate the AI-2 circuit of *Escherichia coli* K12. Specifically, a stochastic Petri net (SPN) model, a mathematical approach succinctly reviewed by Goss and Peccoud (1998) and successfully used for modeling several biological systems (Arkin *et al*, 1998; Matsuno *et al*, 2000; Srivastava *et al*, 2001), was developed for the appearance and disappearance of AI-2 in extracellular fluids of laboratory batch cultures of *E. coli*. This stochastic approach can accommodate large and discrete transitions in its reacting species (Gillespie, 1977; McAdams and Arkin, 1997), and favorably contrasts the deterministic approach, which assumes that the time evolution of a chemically reacting system is continuous. That is, for biological systems, such as genetic regulatory networks with species at very low concentrations (or number) and slow reaction rates, random fluctuations can exist owing to inherent stochastic events. These, in turn, can yield significant variability in system behavior, particularly when modeled stochastically (McAdams and Arkin, 1999; Smolen *et al*, 2000; Gibson and Mjolsness, 2001; Mettetal *et al*, 2006).

Our particular interest was the apparent stimulation of AI-2 due to the presence of glucose, as its presence appears to interfere with QS signaling in *E. coli*. Based on initial simulation and experimental results in LB medium, we investigated several experimental and computational hypotheses related to redistribution of metabolic flux within the AI-2 biosynthesis pathway. The results suggest the existence of an alternative glucose-regulated pathway for autoinducer AI-2 synthesis. We subsequently discovered the conversion of nucleic acid precursor, adenosine, to AI-2 via a pathway other than the well-known Pfs–LuxS pathway. That is, upon interrogating our model simulations and the enzymatic synthesis of AI-2 *in vitro* (Schauder *et al*, 2001; Miller *et al*, 2004), we discovered the existence of an alternative pathway for its synthesis, which is shown here. Other attributes of this SPN approach to investigate bacterial QS are revealed: (1) the stochastic approach formally enables estimation of variance for the simulated concentrations, which can be compared to experimental data, (2) the simulated genetic circuit can be assembled from 'subcircuits' as the complexity and interconnectivity with the rest of metabolism is established, (3) inferences from the literature concerning metabolic flux and other events such as transcription, translation, and biomolecular assembly formation can be tested, and perhaps most importantly, (4) this approach enables a computational framework that allows one to postulate mechanisms and concepts that can ultimately be tested using bacterial genetics.

Results

Model construction

AI-2 biosynthesis and uptake pathways in *E. coli* (Figure 1) have been partially elucidated (Schauder *et al*, 2001; Xavier and Bassler, 2005): AI-2 is derived from *S*-adenosylmethionine (SAM), a major methyl donor in metabolic processes. SAM transfers a methyl group to methyl acceptors by methyltransferases, such as CheR (Yi and Weis, 2002), yielding *S*-adenosylhomocysteine (SAH). SAH is hydrolyzed to *S*-ribosylhomocysteine (SRH) by a nucleosidase, Pfs, with a concomitant release of adenine. LuxS cleaves the thioether linkage of SRH and yields homocysteine and 4,5-dihydroxy-2,3-pentanedione (DPD). It has been reported that AI-2 results from the autocyclization of DPD in at least two additional reactions (Chen *et al*, 2002; Miller *et al*, 2004; Semmelhack *et al*, 2005). SAM, together with diamine and putrescine, is also decarboxylated to form a major triamine, spermidine. This triamine plays an important role in proliferation and differentiation of *E. coli* (Cohen, 1998). This reaction also releases a toxic by-product 5′-thiomethyladenosine (MTA), which is then acted upon by Pfs, yielding adenine and 5′-thiomethylribose (MTR). MTR is reportedly excreted to the medium in *E. coli* (Schroeder *et al*, 1973). The export mechanisms of AI-2 are unknown. Extracellular AI-2 is transported into the cell by an ABC transporter, Lsr (Taga *et al*, 2003; Wang *et al*, 2005a). Its uptake was recently shown to be glucose dependent (Wang *et al*, 2005a). The role of AI-2 beyond regulating its uptake remains unresolved in *E. coli* K12, although many targets have been proposed (DeLisa *et al*, 2001a, b).

An SPN model (Figure 2) was constructed for the AI-2 biosynthesis and uptake pathways (Figure 1). The SPN circuit includes both SAM utilization branches, because Pfs acts on both SAH and MTA, which may enable pathway competition.

Experiments with wild-type *E. coli* have demonstrated that extracellular AI-2 accumulates in the exponential phase and

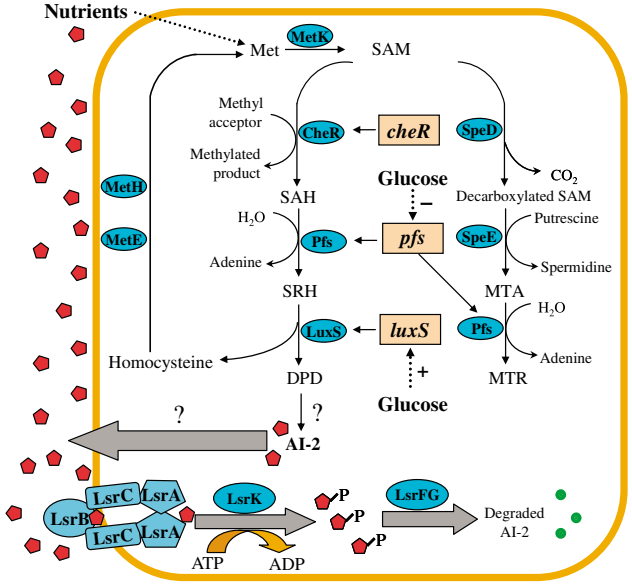

Figure 1 AI-2 synthesis and uptake pathways in *E. coli* (modified from Wang *et al*, 2005a, b).

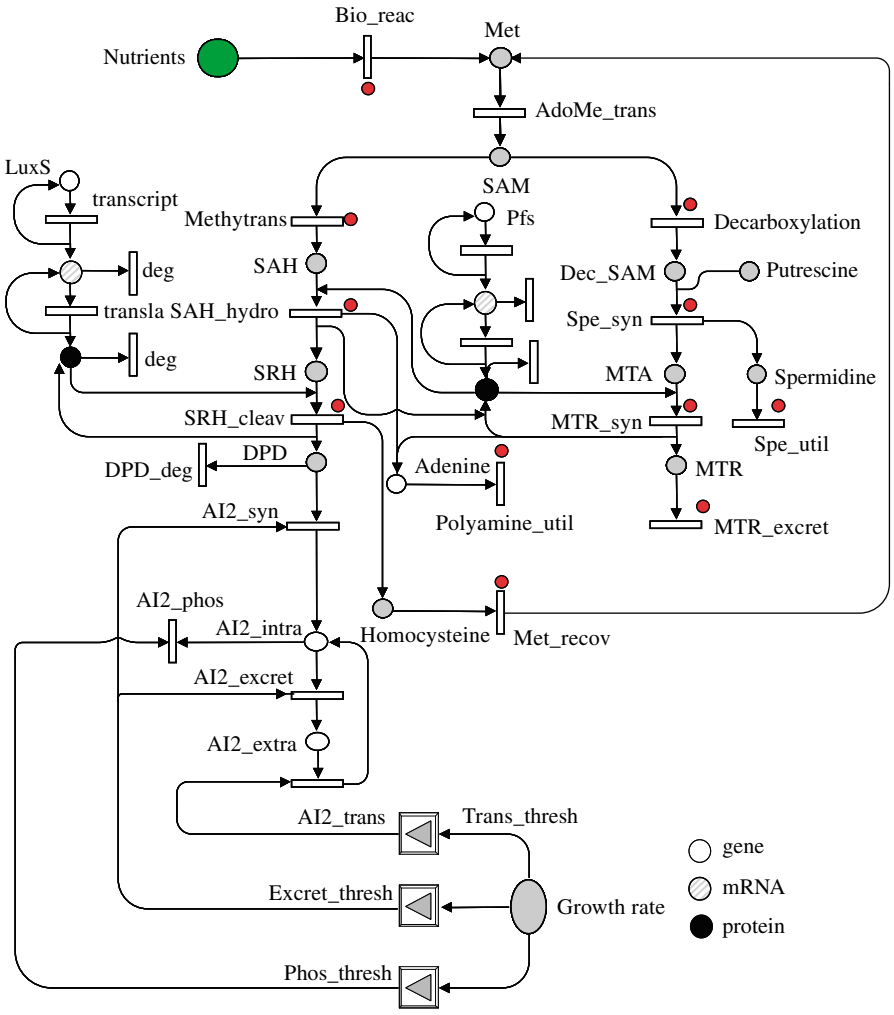

Figure 2 Schematic of SPN for AI-2 genetic circuit (synthesis and uptake). Circles represent places (hollow, genes; dotted, mRNA; solid dark, proteins; gray, other components). Rectangles represent transitions either transcription, translation, or flux-associated reactions (e.g., enzyme-mediated). The reactions indicated by the red circles are altered by the presence of glucose.

then is rapidly depleted at the onset of the stationary phase (Surette and Bassler, 1998). Extracellular AI-2 level is presumed to be a function of synthesis and uptake (Taga *et al*, 2003; Winzer *et al*, 2003; Wang *et al*, 2005a). Our observations, which are consistent with these hypotheses, are that AI-2 is stable in spent culture media devoid of cells (data not shown), so that intrinsic instability of AI-2 is negligible. Thus, for simplicity, we partitioned our SPN so that AI-2 accumulation and uptake are two independent processes. Hence, a quorum signal 'switch' was included to control the AI-2 synthesis and uptake transition. Three input gates (Trans_thresh, Excret_thresh, Phos_thresh) together with a growth rate indicator were used to control the switching process (Figure 2). The instantaneous specific growth rate, which was calculated from experimental data, was used to determine the stage of cell growth and to 'open' specific input gates.

All initial markings and their appropriate references are listed in Table I. For all species, one token represents a single molecule and this was taken as 1 nM concentration (Arkin

Table I Initial markers used in AI-2 circuit

Name	Token number	References
Nutrients	28 350	Pedersen *et al*, 1978
Methionine	2248	Ingraham *et al*, 1983
SAM	10 000	Posnick and Samson, 1999
SAH	320	Hashimoto *et al*, in preparation
SRH	300	Hashimoto *et al*, in preparation
DPD	300	Hashimoto *et al*, in preparation
AI-2	60	Hashimoto *et al*, in preparation
LuxS mRNA	16	Ingraham *et al*, 1983
LuxS protein	400	Neidhardt, 1990
Pfs mRNA	32	Wang *et al*, 2005a
Pfs protein	800	Neidhardt, 1990
Adenine	596	Duerre, 1962
Homocysteine	300	Roe *et al*, 2002
Intracellular AI-2	60	Hashimoto *et al*, in preparation
Extracellular AI-2	60	Hashimoto *et al*, in preparation
Decarboxylated SAM	220	Bowman *et al*, 1973
Putrescine	4400	Cohen, 1998
MTA	296	Duerre, 1962
MTR	180	Schroeder *et al*, 1973
Spermidine	940	Cohen, 1998

Table II Rate constants in AI-2 synthesis and uptake circuit

Reactions	Reaction symbol	Deterministic rate constants	Reference
Bio-reaction[a]	Bio_reac	$0.01\ min^{-1}$	Derived from DeLisa *et al*, 2001a, b
Methionine adenosyl transfer[a]	AdoMet_trans	$0.962\ min^{-1}$	Taylor *et al*, 2002; Newman *et al*, 1998
Methyl transfer[a]	Methytrans	$0.015\ min^{-1}$	Simms *et al*, 1987
SAH hydrolysis[a]	SAH_hydro	$1.32 \times 10^{5}\ M^{-1}\ min^{-1}$	Duerre, 1962; Della Ragione *et al*, 1985
SRH cleavage[a]	SRH_cleav	$4.86 \times 10^{5}\ M^{-1}\ min^{-1}$	Zhu *et al*, 2003
AI-2 synthesis[b,c]	AI2_syn	$6.7 \times 10^{-4} \sim 0.1\ min^{-1}$	Pigman and Isbell, 1968; Isbell and Pigman, 1969 This study, fitted to data
AI-2 excretion[b,c]	AI2_excret	$0.25\ min^{-1}$	This study, fitted to AI-2 data
AI-2 transport[d]	AI2_trans	$0.006–0.03\ min^{-1}$	Li *et al*, 2004
AI-2 phosphorylation[b,c]	AI2_phos	$0.5\ min^{-1}$	This study, fitted to data
SAM decarboxylation[a]	Decarboxylation	$0.055\ min^{-1}$	Wickner *et al*, 1970; Xie *et al*, 1989
Spermidine synthesis[a]	Spe_syn	$8.73 \times 10^{2}\ M^{-1}\ min^{-1}$	Xie *et al*, 1989; Bowman *et al*, 1973
MTR synthesis[a]	MTR_syn	$4.81 \times 10^{3}\ M^{-1}\ min^{-1}$	Duerre, 1962
Spermidine utilization[a]	Spe_util	$2.11 \times 10^{-2}\ min^{-1}$	Kashiwagi *et al*, 1996
LuxS transcription[d,e]	tanscript	$1.25\ min^{-1}$	Records *et al*, 1996; Wang *et al*, 2005a, b
LuxS translation[c]	transla	$0.74\ min^{-1}$	Bremer and Dennis, 1996
Pfs transcription[d,e]	Not denoted	$2.1\ min^{-1}$	Records *et al*, 1996; Wang *et al*, 2005a, b
Pfs translation[c]	Not denoted	$0.54\ min^{-1}$	Bremer and Dennis, 1996
LuxS mRNA degradation[d,f]	deg	$0.03\ min^{-1}$	Kushner, 1996 Fitted to data
Pfs mRNA degradation[d,f]	Not denoted	$0.022\ min^{-1}$	Kushner, 1996 Fitted to data
LuxS protein degradation[c]	deg	$0.012\ min^{-1}$	Assumed
Pfs protein degradation[c]	Not denoted	$0.003\ min^{-1}$	Assumed

Derived deterministic rate constants were transformed into stochastic rate constant; for details, see Supplementary information: Stochastic Petri nets and its algorithm.
[a]Increased 50% owing to the presence of glucose.
[b]Fitted to experimental data in this study, stated in text.
[c]Retained as constant irrespective of glucose.
[d]Adjusted according to experimental data in the presence of glucose.
[e]*luxS* and *pfs* transcription rate fitted to β-galactosidase data in Wang *et al* (2005a); see Supplementary Figure 1.
[f]See Supplementary Figure 1.

et al, 1998). Similarly, all rate constants and their original sources are listed in Table II. Most of these rate constants were collected from literature data of earlier studies (Draper, 1996; Kushner, 1996; Records Jr *et al*, 1996), such as rates of transcription, translation, and metabolic enzyme activity. *LuxS* and *pfs* transcription rates were derived from a typical transcription rate (Records Jr *et al*, 1996) modified by our transcriptional promoter probe data (see Supplementary Figure 1), whereas their mRNA degradation rates were determined from previous reports (Kushner, 1996) together with our NIH image quantified Northern blotting data (see Supplementary Figure 2). These deterministic rate constants were transformed into stochastic constants based on the relationship between mRNA synthesis, degradation, and the cell volume (detailed information is provided in Supplementary information and Supplementary Figure 3).

A base model was constructed for growth in LB medium wherein an AI-2 synthesis rate was found to match our AI-2 data. To be specific, a piecewise constant optimization routine was carried out using an identically constructed ODE model with median output quantities for state variables. The AI-2 uptake rate was based on AI-2 uptake experiments in *luxS* mutant strains MDAI2 and LW3 (Li *et al*, 2004), together with *lsr* transcription rate results (Wang *et al*, 2005a). AI-2 excretion and AI-2 phosphorylation rates were based on intracellular AI-2 experiments, indicating that intracellular AI-2 was insignificant as compared to extracellular levels (data not shown).

ODE parameter optimization was executed using a Matlab® optimization toolbox (http://www.mathworks.com/access/helpdesk/help/toolbox/optim/optim.shtml). AI-2 circuit simulations were run using Mobius on a laptop PC, kindly provided by Dr William Sanders (Center for Reliable and High Performance Computing at the University of Illinois at Urbana-Champaign: http://www.mobius.uiuc.edu/). As our simulations monitor constituents in a single cell, each simulation was terminated at a cell's doubling. For example, during the exponential phase, doubling time was 35 min, the simulation was terminated at 35 min, and constituents' levels were divided by two and set as initial markers for the subsequent run.

AI-2 production in LB medium is partially influenced by Pfs and LuxS

AI-2 activity exists in LB medium of cells grown without glucose, although at a much lower level than with glucose (Wang *et al*, 2005a). Simulations were performed on the AI-2 circuit for cells cultured in LB medium without glucose. During these simulations and because there exist solid literature data on most remaining constants, the AI-2 synthesis rate (k_{syn}) was optimized by minimizing the variance between the simulated results and corresponding experimental data. Hence, the optimized synthesis rate, which enables good agreement with experimental data, is a piecewise constant that increases with time ('LB_sim' in Figure 3A and Table III). That the reaction rate increased with time is an interesting result that will be discussed later. Our decision to optimize the AI-2 synthesis rate as opposed to uptake rate was based on our experimental observations that *luxS* and *pfs* transcript levels

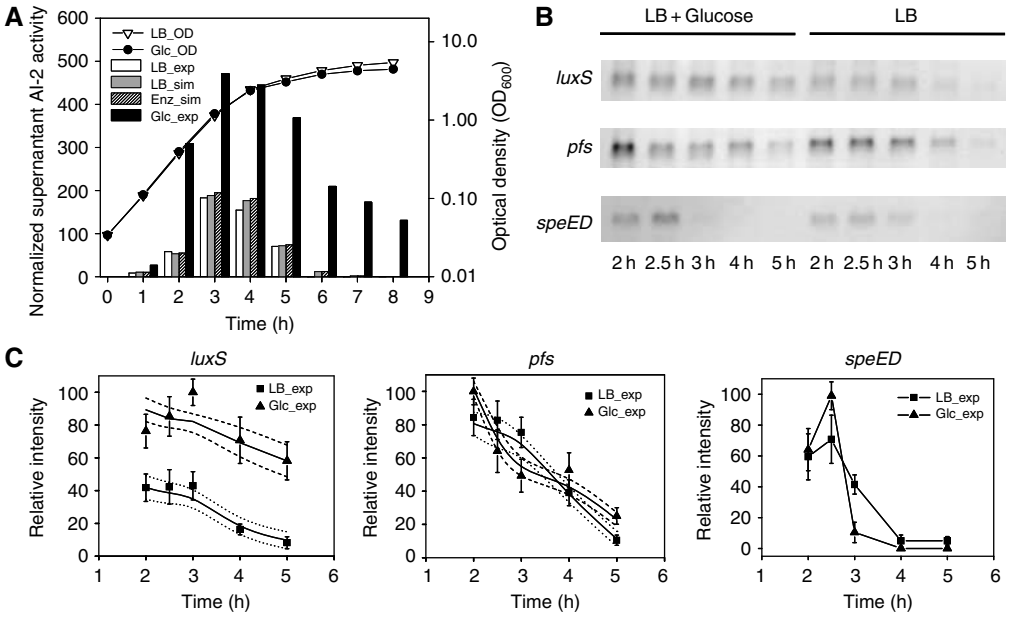

Figure 3 Effects of glucose on AI-2 production and *pfs*, *luxS*, and *speED* mRNA levels. (**A**) Overnight cultures of W3110 were diluted 1:100 in LB and grown to mid-exponential phase, then diluted again into different mediums at an OD_{600} of 0.03. At different time points, aliquots were collected for measurement of OD_{600} (LB, ▽; LB + 0.8% glucose, ●) and AI-2 activity (measured AI-2 in LB, white bar; simulated AI-2 in LB, gray bar; simulated AI-2 with *pfs* and *luxS* mRNA levels influenced by glucose, striped bar; measured AI-2 data in LB + 0.8% glucose, black bar). AI-2 was detected by bioassay using *V. harveyi* BB170 (see Materials and methods); levels shown are representative of three independent experiments. Replicate assays agreed to within 10%. (**B**) Northern blot analyses of *luxS*, *pfs*, and *speED* mRNA levels. (**C**) Densitometric analyses of the Northern blot data shown in (B) and the simulated results (solid and dotted lines) of *luxS* and *pfs* mRNA. The amount of transcript was represented as normalized by the peak levels. Experimental points with error bars are densitometric analyzed data from Northern blots, solid lines represent simulated results, and dotted or dashed lines represent simulation results ± standard deviation. Simulated results of absolute mRNA numbers are transformed into relative level by a constant. Symbols: experimental data in LB, ■; experimental data in LB + 0.8% glucose, ▲; simulated results, solid line; variance of simulated results in LB, dotted line; simulated variance in LB + 0.8% glucose, dashed line.

Table III AI-2 synthesis rate and uptake rate constants in simulations

Growth phase		Synthesis rate in exponential phase (min^{-1}) (k_{syn}, k_{synGlc})						Uptake rate in stationary phase (min^{-1})		
Time/min		35	35	35	35	35	35	70	140	140
Run no.		1	2	3	4	5	6	7	8	9
LB_sim	k_{syn}	6.7e−04	6.7e−04	0.0045	0.0045	0.1	0.1	0.01	0.03	—
Enz_sim	k_{syn}	6.7e−04	6.7e−04	0.0045	0.0045	0.1	0.1	0.006	0.006	0.006
LBOver_sim	k_{syn}	6.7e−04	6.7e−04	0.0045	0.0045	0.1	0.1	0.01	0.03	—
GlcOver_sim	k_{syn}	6.7e−04	6.7e−04	0.0045	0.0045	0.1	0.1	0.006	0.006	0.006
GlcFlx_sim	k_{syn}	6.7e−04	6.7e−04	0.0045	0.0045	0.1	0.1	0.006	0.006	0.006
Glc_sim1	k_{synGlc}	0.0012	0.0012	0.05	0.05	0.05	0.05	0.006	0.006	0.006
Glc_sim2	k_{synGlc}	0.0012	0.0012	0.05	0.05	0.05	0.05	0.006	0.006	0.006

LB_sim represents simulations in LB, Enz_sim represents simulations when *luxS* and *pfs* transcripts change owing to the presence of glucose, and LBOver_sim and GlcOver_sim represent simulations of LuxS and Pfs overexpression in LB without and with glucose, respectively (denoted LuxS_sim or Pfs_sim in Figures 4 and 5, respectively). GlcFlx_sim, Glc_sim1, and Glc_sim2 represent three different simulations in the presence of glucose (Figure 6).

are high during exponential growth and that *lsr* transcription is not initiated until late exponential phase (Wang *et al*, 2005a, b). Hence, synthesis is regulated first, followed by uptake.

It has also been reported that glucose can stimulate AI-2 synthesis. In Wang *et al* (2005a), we demonstrated that the rates of *luxS* transcription were increased owing to the presence of glucose and this increase was mediated by the cAMP–CRP complex. In Figure 3 and Table IV, we show the *luxS*, *pfs*, and *speED* mRNA levels, detected by both Northern blot and qRT–PCR, in cells grown with and without glucose. Interestingly, the Northern data suggest a two- to seven-fold increase in *luxS* mRNA in glucose-grown cells, whereas the qRT–PCR data track the transcription rate data obtained previously (∼1.5- to 2-fold increase; Wang *et al*, 2005a). Because of the apparent variability in mRNA data based on the two measurement techniques, the rates of *luxS* and *pfs* transcription were calculated twice, corresponding to both data sets (Table IV) and both sets of simulation results indicated only a 10% increase in calculated AI-2 (Figure 3A, only 'Enz_sim' is shown here for the Northern data). Importantly, irrespective of the mRNA quantities, the experimentally observed AI-2 levels were three-fold higher than that predicted by SPN. Not seen in these simulations are the

Table IV *luxS* and *pfs* mRNA level from real-time PCR and comparison to quantified Northern blot data

Gene	Time (h)	Real-time PCR fold change		Relative mRNA level (mRNA in Glc divided by mRNA in LB)			
		LB	Glc	Real-time PCR		Quantified Northern blot	
				Exp.	Sim.	Exp.	Sim.
luxS	2	0.47±0.12	0.75±0.20	1.60	1.21	1.82	1.93
	2.5	0.62±0.10	0.906±0.13	1.44	1.76	2.02	2.20
	3	1.38±0.29	1.00±0.11	0.72	1.45	2.32	2.22
	4	1.11±0.03	1.97±0.19	1.79	1.68	4.34	4.30
	5	0.84±0.14	1.87±0.20	2.23	2.48	7.10	5.98
pfs	2	0.65±0.10	0.72±0.04	1.10	1.00	1.18	1.26
	2.5	0.75±0.02	0.86±0.11	1.14	1.23	0.77	0.92
	3	0.99±0.19	1.00±0.12	1.01	1.42	0.65	0.78
	4	0.90±0.13	1.27±0.16	1.41	1.39	1.34	1.22
	5	0.52±0.08	0.95±0.15	1.84	1.68	2.39	2.04

'Glc' represents LB with 0.8% glucose, 'Exp.' represents experimental data, and 'Sim.' represents simulation data. RT–PCR results are normalized to 3 h time point (underlined).

estimated variances calculated by the stochastic model. In particular, the AI-2 variance was less than 5% of the mean throughout the simulation period. The most widely varied constituents were indeed the levels of *luxS* and *pfs* mRNA (~16%), as indicated in Figure 3C, which roughly correspond to the standard errors associated with the Northern blot measurements.

These results suggest that changes in the levels of these key enzymes do lead to the stimulation of AI-2 production, but at levels much less than that needed to rectify simulation with experimental results from cultures containing glucose.

In order to test this enzyme dependence further, the AI-2 circuit was experimentally perturbed by *luxS* and *pfs* overexpression. IPTG-inducible expression vectors for the production of LuxS and Pfs were introduced into W3110 cells, which, in turn, were grown in the presence and absence of glucose. First, in the absence of glucose and consistent with Figure 3, *luxS* overexpression resulted in only a small AI-2 increase (about 16%) relative to the control (plasmid without *luxS* insertion) (Figure 4A). Interestingly, *pfs* overexpression resulted in no clear trend and no appreciable difference relative to the control (plasmid without *pfs* insertion) (Figure 4A). In order to mimic the effects of *luxS* and *pfs* overexpression on the AI-2 SPN, their transcription rates were increased 200-fold. This is a much more severe test of the reaction network's dependence on LuxS and Pfs expression than the simulations above (Figure 3). The resultant LuxS and Pfs protein levels were calculated to be around 200- to 300-fold higher than that of wild-type cells in the mid-exponential phase (Figure 4D). Although not shown, the levels of these enzymes in the wild-type cells did not change significantly with time (i.e., they roughly correspond to transcript levels in Figure 3C). The corresponding calculated AI-2 levels were raised by less than 10% (Figure 4C). These simulation results corroborate the experimental findings that *luxS* and *pfs* overexpression only minimally influences AI-2 production in LB medium without glucose.

In Figure 5A, cells overproducing each of the synthases in the presence of glucose exhibited significantly higher levels of AI-2. In the case of LuxS, the increase was more immediate than with Pfs. The levels of LuxS and Pfs in these overproducing cells were estimated to be 200-fold greater than that of uninduced controls (quantified results in Figure 5D). By increasing *luxS* mRNA (owing to the presence of glucose) in the network, and performing similar *luxS* or *pfs* overexpression simulations as stated in LB medium, we saw only similarly increased AI-2 levels (less than 10%, data not shown).

Taken together, these simulations have demonstrated that the expression level of LuxS and Pfs enzymes cannot notably enhance AI-2 production. However, experiments have clearly demonstrated that overexpression of LuxS and Pfs can effectively increase AI-2 production when glucose is present. This discrepancy suggests that the increase in AI-2 production due to the presence of glucose may result from factors other than LuxS and Pfs, in ways that have yet to be revealed. This is partially explored by examining carbon flux through the biosynthesis pathways.

Glucose provides enhanced flux through the LuxS synthesis pathway

Based on the work of Holms (1996) on flux analysis of *E. coli* grown with different carbon sources and the work of Oh and Liao (2000), the presence of glucose and varied carbon sources can significantly enhance the flux through central metabolic pathways. According to their data, a 50% increase in the flux of material through the AI-2 circuit due to the presence of glucose is reasonable. Hence, we carried out several 'what if' simulations, whereby metabolic fluxes other than the AI-2 synthesis rate from DPD and its uptake were upregulated 50% as compared to that without glucose. In the first set of simulations (GlcFlx_sim; Figure 5C), the two-fold increase of *luxS* mRNA due to glucose was included, but without overexpression of *luxS* and *pfs*. The calculated AI-2 increased 35% over that without glucose. The addition of *luxS* and *pfs* overexpression to the case of increased metabolic flux only marginally increased AI-2 levels (LuxS_sim, Pfs_sim in Figure 5C).

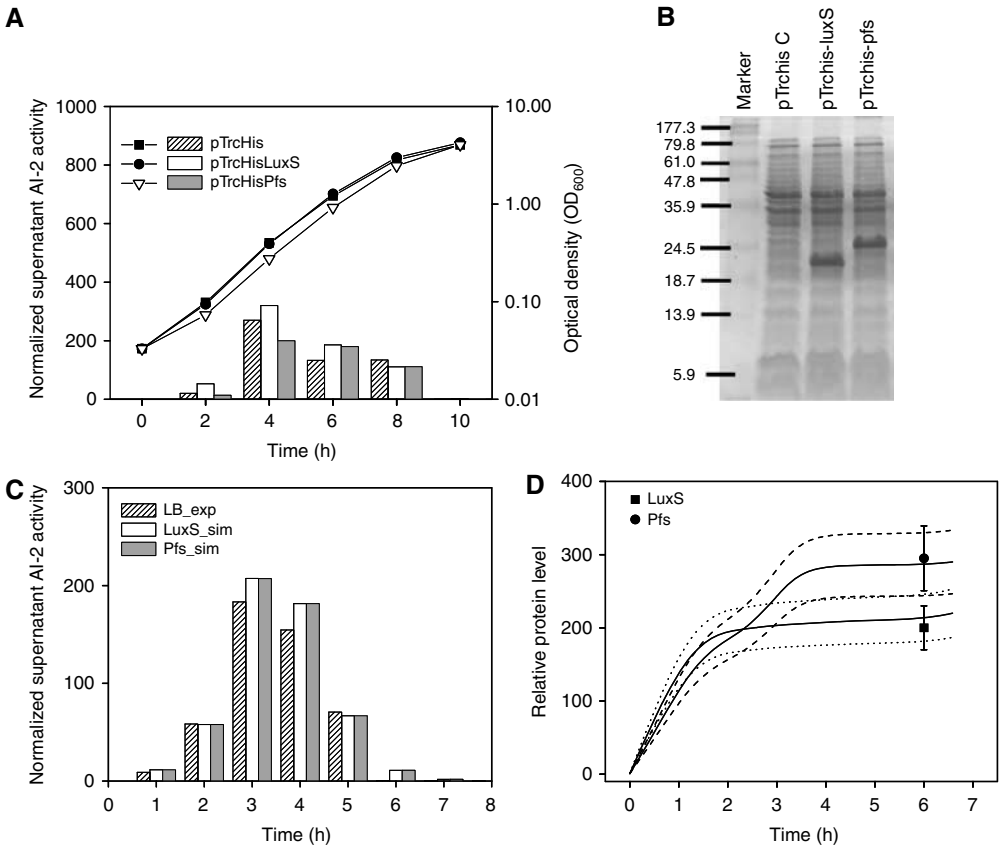

Figure 4 *luxS* and *pfs* overexpression partially influences AI-2 formation in LB medium. (**A**) Overnight cultures were diluted 1:100 in LB medium; IPTG was added to cultures at 1 mM (*trc* promoter) at time zero. Aliquots were collected for measurement of OD_{600} (rectangle, circle, and triangle) and AI-2 activity (bar). AI-2 was detected by using *V. harveyi* BB170. AI-2 activities shown are representative of three independent experiments. Replicate assays agreed to within 10%. (**B**) Overproduction of LuxS and Pfs was confirmed by SDS–PAGE using samples taken at 6 h. (**C**) Simulation results of *luxS* and *pfs* overexpression are compared to experimental data from LB cultures; corresponding protein levels are indicated in (**D**). Relative protein level was obtained from the simulated protein molecule at time *t* divided by the initial protein molecule at initial time t_0. The relative experimental data were obtained from the image quantified protein molecule divided by the same initial protein molecule as in simulations. Symbols in (C): AI-2 activity experimental data in LB, striped bar; luxS overexpression simulation results, white bar; *pfs* overexpression simulation results, gray bar. Symbols in (D): LuxS and Pfs levels quantified using NIH image (LuxS level, ■; Pfs level, ●). Solid lines represent simulated LuxS and Pfs, dotted lines represent mean values ± variance of simulated LuxS, and dashed lines represent the same for Pfs.

In Figure 5A, cells overproducing each of the synthases in the presence of glucose exhibited significantly higher levels of AI-2. In the case of LuxS, the ~2-fold increase was more immediate than that with Pfs. In Figure 5B, the level of LuxS and Pfs in these overproducing cells was estimated to be 200-fold greater than that of the uninduced controls (quantified results are depicted in Figure 5D). Simulations with glucose present (i.e., higher initial *luxS* mRNA) predict that overexpression of both *luxS* and *pfs* enhances AI-2 production over the LB SPN calculations, but by less than or near two-fold (Figures 5C and 4C). Interestingly, the simulated levels of LuxS was higher than that without glucose (Figures 5D and 4D). It is again noteworthy that the LuxS and Pfs protein levels were within the variances calculated by the SPN. Also, experimental observations indicated a more immediate response in the case of LuxS overexpression, yet there was no distinct difference in calculated AI-2 even though the calculated LuxS level appeared to increase more quickly than Pfs. We note that in experiments, the peak AI-2 levels were similar in both overexpression cases (~800 normalized activity units; Figure 5A), and roughly 1.5-fold higher than the + glucose case without enzyme overexpression (Figure 5A). That the SPN captured the relative increase in AI-2 (~1.5- to 2-fold) due to the enzyme overexpression in the presence of glucose was both interesting and noteworthy, but our simulations still missed the overall enhancement resulting from glucose itself. Most importantly, an approximately 250- to 500-fold increase in each enzyme resulted in only a maximum two-fold increase in AI-2.

Trends in all of the above simulations are consistent with our experimental results and a previous report that flux increases stimulate AI-2 production (Posnick and Samson, 1999). Because the simulated AI-2 levels remained much lower than the experimental data, we hypothesized that the rate of AI-2 synthesis from DPD was itself a function of glucose, with an as yet to be determined functional form. This has varied ramifications, as will be discussed.

In order to set up further simulation experiments, we performed a piecewise linear optimization analysis to 'find' the AI-2 synthesis rate constant (k_{synGlc}) that best matched the experimental data with glucose present. As our simulation rate constants are most grounded in events associated with

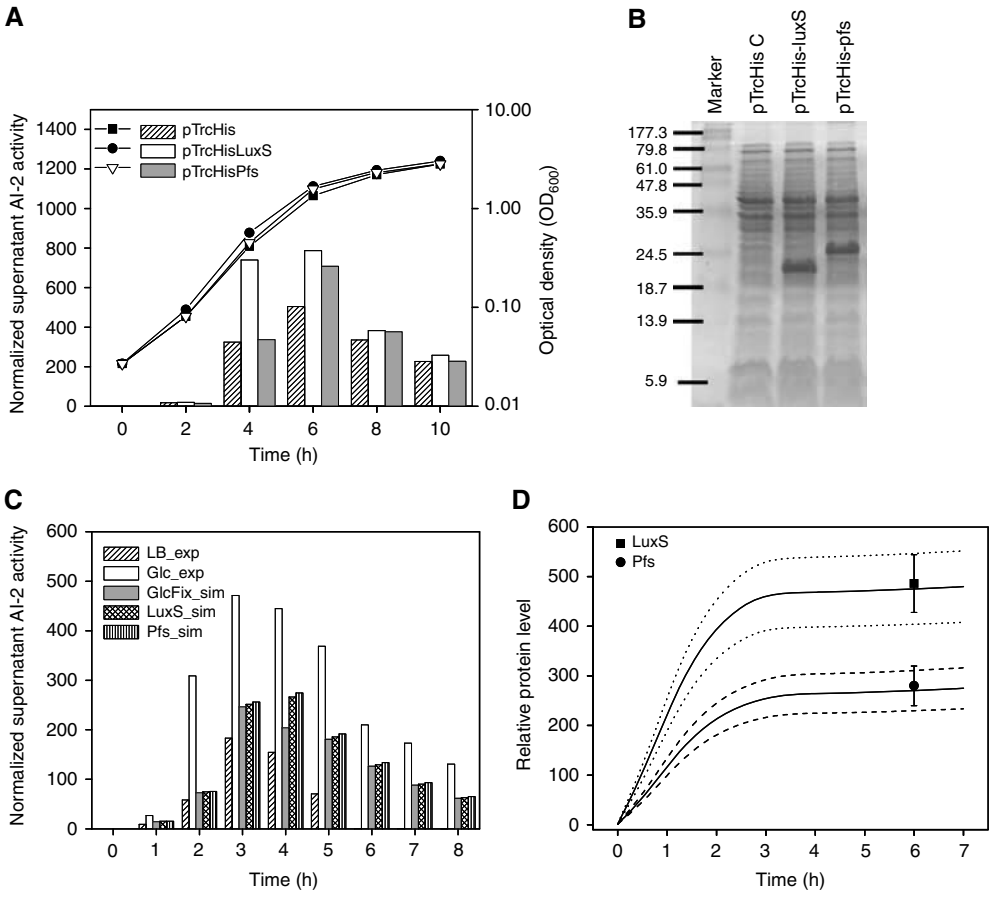

Figure 5 *luxS* and *pfs* overexpression affects AI-2 formation in the presence of glucose. Overnight cultures were diluted 1:100 in LB + 0.8% glucose medium and IPTG was added to cultures at 1 mM (*trc* promoter) at time zero. (**A**) Aliquots were collected for OD_{600} (rectangle, circle, and triangle) and AI-2 activity (bar) measurement. (**B**) Overproduction of LuxS and Pfs was confirmed by SDS–PAGE using samples taken at 6 h. AI-2 was detected using *V. harveyi* BB170 (Materials and methods). AI-2 activities shown are representative of three independent experiments. Replicate assays agreed to within 10%. (**C**) Simulation results of *luxS* and *pfs* overexpression on AI-2 production in the presence of glucose. (**D**) Corresponding protein levels are indicated (fold-increase relative to control). Relative protein level was obtained as described in Figure 4. Symbols in (C): AI-2 activity experimental data in LB, striped bar; AI-2 activity experimental data in LB + 0.8% glucose, white bar; simulation results of 50% fluxes increase owing to the presence of glucose, gray bar; simulated AI-2 level of *luxS* overexpression in LB + 0.8% glucose, crossed bar; AI-2 simulation results of *pfs* overexpression in LB + 0.8% glucose, vertical bar. Symbols in (D): NIH image quantified experimental LuxS (■) and Pfs (●) levels. Solid lines represent simulated LuxS and Pfs levels, broken lines represent mean values ± variance (LuxS, dotted; Pfs, dashed).

transcription, translation, and flux in the enzyme-mediated reactions, we optimized the AI-2 synthesis rate under the condition of 50% increased metabolic flux. In Figure 6, the corresponding best-fit simulation results for the glucose case are, as expected, in close agreement with the data (Figure 6, Glc_sim1). The experimental results and the previous GlcFlx_sim from Figure 5C are also included. In Table III, the corresponding synthesis rates for the conversion of DPD to AI-2 increased ~10-fold over the previous case during the period of maximum AI-2 increase (2–3 h). The maximum difference between calculated results and measurements was less than 15%.

A second simulation was run, in which the 'optimized' AI-2 synthesis rate was run without enhanced metabolic flux (Figure 6, Glc_sim2). This tests whether the influence of glucose on the well-studied synthesis pathway is the potential problem in our SPN circuit. The results are again significantly different from the experiments, reinforcing the suspicion that our model construction from DPD to AI-2 is flawed. That is, the net result of these simulations demonstrated that increases in 'upstream' metabolic flux stimulate AI-2 production, but that the apparent non-enzymatic conversion of DPD to AI-2 may be the basis for discrepancy. One explanation is that there are alternative pathways other than those well documented (as shown in Figure 1) for AI-2 synthesis. These may be induced and/or undergo a dramatic flux increase due to the presence of glucose.

Alternatively, when cells enter the stationary phase, AI-2 uptake takes place. As stated above, the AI-2 uptake rate was determined in the initial model based on LB medium (Li *et al*, 2004). However, in the presence of glucose (0.8% glucose in LB), AI-2 uptake was observed to be slower as compared to that without glucose, owing to the CRP-mediated repression of glucose on AI-2 uptake (Taga *et al*, 2003; Wang *et al*, 2005a). A reduced uptake rate would increase the extracellular AI-2 level. Although not noted earlier, a revised AI-2 uptake rate (reduced by more than 40%) was used in the above simulations representing glucose addition (Table III).

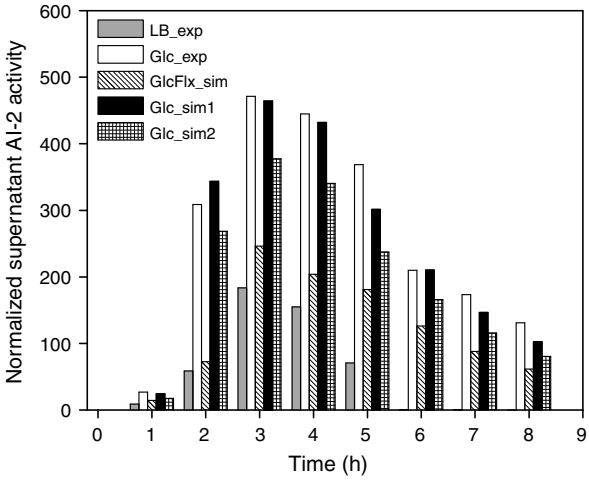

Figure 6 Glucose affects AI-2 formation by increasing fluxes through AI-2 pathway and modulating AI-2 synthesis rate. Symbols: AI-2 experimental data in LB, gray bar; AI-2 experimental data in LB + 0.8% glucose, white bar; 'GlcFlx_sim' (striped bar) denotes results for 50% increase in the flux of reactions denoted by red circles in Figure 2; 'Glc_sim1' (black bar) denotes results of optimized AI-2 synthesis rate together with a 50% increase in the flux of reactions denoted by red circles in Figure 2; 'Glc_sim2' (rectangular bar) denotes the results of optimized AI-2 synthesis rate only.

However, when the AI-2 uptake rate constant was lowered 10-fold to reflect nearly complete repression of uptake, there was no depletion of AI-2 level in the supernatant (not shown here). This is inconsistent with the experimental results, which clearly demonstrated AI-2 uptake, even in cells devoid of the active *lsr* uptake transporter (Wang *et al*, 2005a). A further modification is envisioned wherein uptake and synthesis are coordinated so that cessation of synthesis ends after AI-2 uptake begins. Our experimental evidence with *lsrK* knockouts however demonstrates that AI-2 synthesis indeed ends at switch times or conditions as indicated, and AI-2 levels remain the same during the stationary phase (Wang *et al*, 2005a). If there were still AI-2 synthesis under the condition without any uptake, we would see a continually increased AI-2 activity.

Is conversion of 4,5-dihydroxy-2, 3-pentanedione a high-flux reaction?

We were interested in the report of Almaas *et al* (2004), which suggests that the biochemical activity of metabolism is dominated by a few high-flux backbone reactions embedded in a network of mostly small-flux reactions. They reported that only high-flux reactions go through noticeable flux changes, whereas low-flux reactions undergo small shifts. Based on this, we speculated that there may be hidden high-flux reactions among the AI-2 synthesis pathways. As stated above and confirmed by experiment and simulation, the increase in transcription and/or translation of *luxS* and *pfs* cannot enhance AI-2 production significantly. Further, a dramatic increase, more than 200-fold, in upstream precursor, SAM, only stimulated an approximate 60% AI-2 increase (Posnick and Samson, 1999).

This turned our attention to post-LuxS processing (the correct cyclization of DPD; Miller *et al*, 2004), which is reported to be a result of mass action kinetics as opposed to an enzyme- or chaperone-mediated event. We wonder whether this conversion, putatively in the cell cytoplasm, could proceed without any biological assistance. After many efforts including our own, biologically produced AI-2 has never been isolated without further biological assistance such as binding to a cognate receptor (Chen *et al*, 2002; Meijler *et al*, 2004; Miller *et al*, 2004; Semmelhack *et al*, 2004, 2005). Similarly, pure DPD has also not been reported, instead 'pure' DPD is a mixture of DPD together with its two anomers at their low concentration (Meijler *et al*, 2004). The mechanism by which AI-2 is formed from its precursor, DPD, remains enigmatic in *E. coli*. Hence, we predicted that the reaction from DPD to AI-2 potentially serves as a hidden high-flux reaction in the AI-2 QS network.

During our 'fit' simulations, the AI-2 synthesis rate increased significantly with the growth of cells. This rate constant represents the net reaction rate from DPD to AI-2; our results clearly indicated that the reaction from DPD to AI-2 has a strong impact on AI-2 level. Furthermore, mechanistically, DPD is putatively the principal molecule from which all bacterial AI-2 is derived (Miller *et al*, 2004; De Keersmaecker *et al*, 2005; Semmelhack *et al*, 2005). Because of the apparent impact of this reaction on AI-2 level, we performed additional simulations (Figure 7) to differentiate potential mechanisms that contribute to this pathway. First, we intentionally reduced the AI-2 synthesis rate constant, k'_{synGlc}, to gauge its importance on AI-2 formation from DPD in the case of glucose-mediated flux increases and Pfs/LuxS synthase mRNA changes (DPD_sim1; Figure 7A). This reduced synthesis rate was ~3-fold lower than the 'optimized' AI-2 synthesis rate (k_{synGlc}) in the earlier glucose simulations (Glc_sim1, Glc_sim2 in Figure 6), but was maintained ~3-fold higher than the initial simulations (e.g., GlcFlx_sim in Figure 5). The resultant AI-2 level was much lower than that from our observations, as expected. This case represents a logical extension of our experimental findings, and is included to represent an intermediate level of enhanced reaction (Figure 7A and Table V).

Second, 'DPD_sim2' was carried out by maintaining an ~20% higher DPD concentration than the previous cases, but with the same AI-2 synthesis rate constant k'_{synGlc} as in DPD_sim1. In Mobius, this is accomplished by redefining the input function of DPD tokens, so that upon transition or 'firing', the number of DPD tokens was not reduced by one and was instead unchanged. This case represents a situation where other reactions produce DPD from as yet unidentified pathways (indicated by a side entry reaction in DPD_sim2 of Figure 7C). The simulated results were in good agreement with our experimental data.

Third, 'DPD_sim3' (same as Glc_sim1 in Figure 6) was performed under the original DPD configuration with the 'optimized' synthesis rate constant, k_{synGlc}. This simulation represents the situation where the rate constant from DPD to AI-2 was increased 40-fold over time (indicated by the thick arrow in Figure 7C). As noted above, the simulations fit the data well.

The AI-2 synthesis rates for all three simulations are listed in Table V. The DPD levels (relative to the initial tokens) under these three different conditions are depicted in Figure 7B along

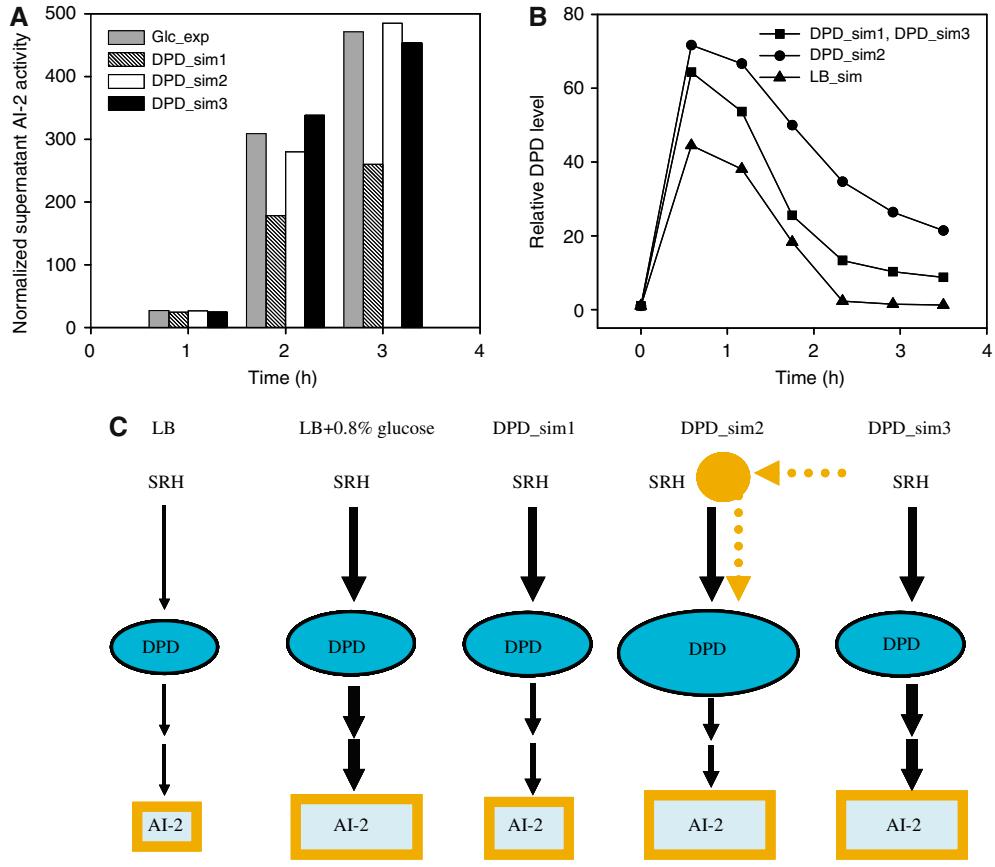

Figure 7 Modulating flux from DPD to AI-2 significantly affects AI-2 formation. (**A**, **B**) 'DPD_sim1' denotes base model for DPD and a low AI-2 synthesis rate, k'_{synGlc}. 'DPD_sim2' denotes artificially high DPD level with low AI-2 synthesis rate, k'_{synGlc} (this is the case for high flux through DPD to AI-2). 'DPD_sim3' denotes a normal DPD level with 'optimized' AI-2 synthesis rate k_{synGlc}. 'Glc_exp' denotes experimental data with glucose present; 'LB_sim' denotes simulation results for base case in LB media. (**C**) Schematic of AI-2 synthesis from Pfs product, SRH. The relative areas of DPD and AI-2 represent, but are not scaled to their respective quantities. Dashed arrows represent unknown pathways. Relative DPD level was obtained from the simulated DPD molecule at time t divided by the initial DPD molecule at initial time t_0.

Table V AI-2 synthesis rate constant comparison under simulations with different DPD levels

Growth phase		Synthesis rate in exponential phase (min^{-1}) (k_{synGlc}, k'_{synGlc})						Uptake rate in stationary phase (min^{-1})		
Time/min		35	35	35	35	35	35	70	140	140
Run no.		1	2	3	4	5	6	7	8	9
DPD_sim1	k'_{synGlc}	0.0012	0.0012	0.015	0.015	0.015	0.015	0.006	0.006	0.006
DPD_sim2	k'_{synGlc}	0.0012	0.0012	0.015	0.015	0.015	0.015	0.006	0.006	0.006
DPD_sim3	k_{synGlc}	0.0012	0.0012	0.05	0.05	0.05	0.05	0.006	0.006	0.006

DPD_sim3 is the duplicate of previous Glc_sim1.

with the base LB case. An initial rapid transient was observed in which the +glucose cases reached a significantly higher level. The ~3-fold increase in AI-2 synthesis rate constant (k'_{synGlc}) coupled with an artificially increased DPD level (DPD_sim2) resulted in a close fit with the experimental data. An additional 3-fold increase in the AI-2 synthesis rate constant, k_{synGlc}, coupled with the original DPD conditions also resulted in a good fit of the experimental data (DPD_sim3).

Readily apparent from these simulations is that AI-2 production can be made to match experiments either by elevating the intracellular DPD level or by increasing the AI-2 synthesis rate constant from DPD. Our simulations are consistent with either an alternative source of DPD or an enhanced reaction rate from DPD, both of which served to explain the increased AI-2 level in the presence of glucose.

In total, our simulations suggest that in order to accurately simulate the AI-2 level in the extracellular medium, the reaction from DPD to AI-2 must increase in time, and in the presence of glucose, must increase an additional 10-fold beyond the base case. Or alternatively, the reaction rate must increase ~3-fold in concert with a significantly increased level of intracellular DPD. All of these scenarios suggest that the

reaction from DPD may be a high flux reaction that varies significantly in rate.

Experiments demonstrating existence of alternative AI-2 synthesis pathways

In order to probe this hypothesis experimentally, we turned to the substrates and by-products of this two-enzyme AI-2 synthesis system. In particular, we considered the potentially broad substrate specificity of Pfs (it participates in both reaction pathways; Figure 1). We incubated soluble cell extracts and imidazole-eluted enzyme fractions of NC13 (a *pfs* null mutant) and DH5α (a *luxS* frameshift mutant) with and without the overexpression of His-Pfs and His-LuxS, respectively, with adenosine. Then, we assayed for BB170-responsive autoinducer AI-2 activity (Figure 8). Interestingly, all reactions of soluble cell extracts incubated with adenosine were found to induce BB170 cells to produce luminescence, irrespective of the absence of His-Pfs or His-LuxS. Further, imidazole-eluted fractions of Co^{2+} resin-immobilized His-Pfs or His-LuxS induced no or negligible amounts of luminescence when reacted with adenosine (positive controls with SAH showed significant AI-2 production). Reaction of soluble cell extracts with Co^{2+}-immobilized enzymes but without adenosine induced negligible luminescence and, moreover, adenosine itself showed no independent autoinducer activity on BB170 cells (data not shown). HPLC analysis revealed no reaction of adenosine with either purified Pfs or LuxS (data not shown).

Because AI-2 activity is made from cell extracts in the absence of Pfs in one case and LuxS in the other, and because the purified enzyme fractions yield no autoinducer from adenosine, we conclude that adenosine is not a substrate for either enzyme. Instead, other enzymes or precursors in soluble cell extracts are likely responsible for converting adenosine to a BB170-responsive autoinducer.

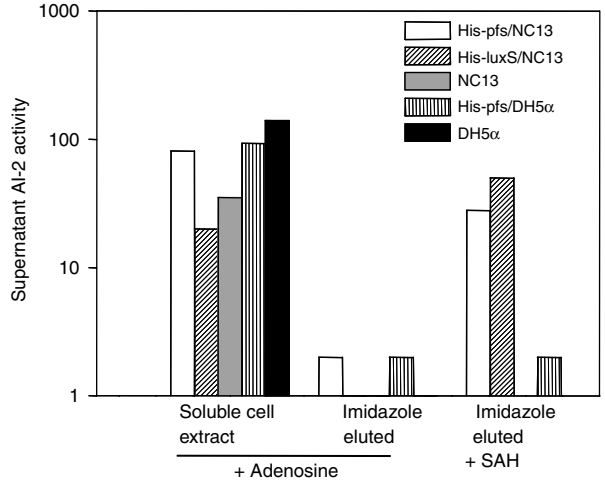

Figure 8 AI-2 produced from reactions with substrates adenosine and SAH, with cell extracts as indicated. *V. harveyi*-responsive autoinducer activity was measured after reaction of (1) adenosine with soluble extracts of cells overexpressing His-Pfs or His-luxS or imidazole-eluted fractions of purified His-pfs or His-luxS, and (2) reaction of SAH with purified His-Pfs or His-LuxS. Strains NC13 and DH5α are Pfs and LuxS mutants, respectively.

In further studies of *in vitro* AI-2 synthesis, we found that LuxS could act on SAH directly, producing AI-2 activity (Hashimoto *et al*, in preparation). This was not revealed *in vivo*, as conditioned medium from *pfs* null mutants was devoid of AI-2. Nevertheless, several preparations of LuxS were shown to convert SAH to AI-2 activity. We note that eukaryotes convert SAH to adenosine and homocysteine via SAH hydrolase in one step. Although the products of LuxS-mediated SAH degradation do not include adenosine, the potential for enzymatic cross-reactivity with SAH was an interesting finding. Thus, we speculated that *E. coli* may convert adenosine to AI-2 via a non-LuxS pathway. Interestingly, an alternative pathway for DPD and AI-2 formation was found in tomato, where DPD was formed from D-ribulose-5-phosphate spontaneously. D-Ribulose-5-phosphate was synthesized from D-ribose-5-phosphate and the enzyme is responsible for this conversion is ribose-5-phosphate isomerase (Hamada *et al*, 2003; Hauck *et al*, 2003). In a related work, LuxS-independent AI-2 formation was reported from a sugar phosphate, ribulose-5-phosphate, which exhibited stronger induction of the AI-2-specific reporter strain than a spontaneously formed product 4-hydroxy-5-methyl-furanone from DPD (Hofmann, 1998; Tavender *et al*, 2004). In *E. coli*, adenosine can be salvaged to ribose-1-phosphate through pentose phosphate metabolism, whereas ribose-1-phosphate can be converted to ribose-5-phosphate by phosphopentomutase, then ribose-5-phosphate can be isomerized to ribulose-5-phosphate (Sorensen and Hove-Jensen, 1996). The existence of AI-2 from reaction of adenosine with cellular extracts from either *luxS* or *pfs* mutant may then be the result of a series of reactions of adenosine salvation through ribose metabolism. The reconstruction of this pathway *in vitro* is currently underway.

These experimental findings demonstrate that alternative pathways for autoinducer AI-2 formation exist, and our simulation results suggest that their rates are dependent on glucose. It is uncertain whether all these alternative pathways are related to DPD, whose autocyclization is putatively responsible for AI-2 formation (Schauder *et al*, 2001; Chen *et al*, 2002; Miller *et al*, 2004). We favor the existence of DPD-related alternative pathways for AI-2 formation because (1) chemically synthesized DPD was shown to be a strong inducer of AI-2 activity (Meijler *et al*, 2004; De Keersmaecker *et al*, 2005) and (2) all the identified autoinducers were shown to be derived from DPD (Miller *et al*, 2004; Semmelhack *et al*, 2005). In summary, these reports indicate that alternative pathways to AI-2 other than those well documented exist, among which ribose sugar phosphates may be involved. We suggest that the dramatic AI-2 increase in the presence of glucose may be attributed to the prevalence of sugar phosphates in cells grown with glucose or to other ill-defined pathways in *E. coli*.

Discussion

An SPN model was employed to simulate AI-2 QS circuit in *E. coli*. Simulation results were in good agreement with experimental data, particularly for the case of cells grown in LB media without glucose. The appearance and disappearance of AI-2 in the growth medium was directly calculated based on the known biochemical pathways. The mRNA levels of two

important AI-2 synthases (Pfs and LuxS) were accurately depicted. Moreover, the SPN model predicted both the relative increase in the synthase level as well as the relative insensitivity of AI-2 due to this perturbation. It is also noteworthy that the variances calculated by the SPN were similar to the experimental errors associated with several of our measurements (e.g., mRNA levels, LuxS, Pfs levels). By representing this network in the Mobius simulation environment, one can with relative ease add additional structure and complexity, in order to generate testable hypotheses regarding the predicted outcomes.

As an example, we speculated that increased metabolic flux from the addition of glucose to the growth media would be required to enhance AI-2 production (additional synthases would be insufficient). This was validated by the simulation results, where a 50% increase in flux resulted in ~35% AI-2 production (Figure 6). More importantly, our simulations led to a hypothesis that a significant increase in AI-2 production from cells grown with glucose may have resulted from unrevealed alternative pathways involving compounds such as sugar phosphates or other unknown regulators modulating the flux to AI-2 (Sperandio *et al*, 2003; Tavender *et al*, 2004). In separate experimental tests using cell extracts, we confirmed that adenosine can be converted to AI-2 from both *pfs* and *luxS* mutants, demonstrating for the first time a biological route to AI-2 from adenosine. It is likely, however, that this particular pathway is masked *in vivo*, as the addition of adenosine to wild-type cells does not stimulate AI-2 production (not shown). Our results would suggest that the presence of glucose instead alters the relative flux between these pathways.

We also showed that the level of DPD plays an important role in AI-2 formation. This is consistent with recent reports indicating that DPD is the core molecule for AI-2 formation (Meijler *et al*, 2004; Semmelhack *et al*, 2004, 2005). Our simulations showed that AI-2 production can be effectively influenced by modulating the flux from DPD to AI-2, which can be achieved by increasing the concentration of DPD or by enhancing the AI-2 synthesis rate constant. However, we note that DPD is reportedly highly reactive and unstable (Winzer *et al*, 2002; Meijler *et al*, 2004). Therefore, we believe that it is unrealistic that a cell can maintain a high DPD level without chaperones or other compartmentalization moieties for enabling stimulated AI-2 synthesis. It has been demonstrated *in vitro* that AI-2 can be derived from DPD and its two ring-closed equilibrium anomers without enzyme catalysis, suggesting that the species specificity is derived at the level of the cognate receptor (Meijler *et al*, 2004; Semmelhack *et al*, 2004, 2005). In the absence of a DPD-specific efflux transporter, it is likely that DPD undergoes intramolecular nucleophilic attack by the hydroxyl group on the carbonyl carbon *in vivo*, producing five-membered cyclic furanose anomers. These two anomers go through mutarotation, like other cyclic sugar anomers, and the equilibrium between these two anomers can be shifted owing to addition of the boric acid, which can stimulate the production of *Vibrio harveyi* AI-2 anomer and repress the release of the *Salmonella typhimurium* AI-2 anomer (Miller *et al*, 2004).

Early in the 1960s, Pigman and Isbell (1968) reported that ring-closure reactions from unstable acyclic chain forms are extremely rapid, with reaction rate constants as high as 10^2 per minute. They also noted that the maximum mutarotation rate between the two cyclic anomers is only about 10^{-2} per minute. At the same time, they noted that if there are no factors other than water to facilitate anomer mutarotation, the reaction rate is very slow, of the order 10^{-3} per minute (Isbell and Pigman, 1969). They further pointed out that this slow mutarotation rate can be increased by factors such as acids or bases. Therefore, we speculated that the ring-closure reaction (from DPD to cyclic AI-2 precursors) is a fast reaction, whereas the mutarotation rate of different cyclic AI-2 anomers is the slow step for forming specific quorum-sensing AI-2 signal. Our initial AI-2 synthesis rate was based on a slow sugar cyclic anomers' mutarotation rate under water's catalysis, which is in the range of the reported literature data. During the simulations with glucose, we increased the initial AI-2 synthesis rate to match experimental data. However, according to the current knowledge of the AI-2 synthesis process, the conversion of DPD to AI-2 is determined exclusively by mass action kinetics at a presumably constant temperature, pressure, pH, etc. Hence, it is infeasible that the AI-2 reaction rate from DPD, as described here, will increase so dramatically unless the concentration of DPD within the cell increases concomitantly, which is seemingly also infeasible.

In order to rectify these discrepancies, it is logical that other enzyme- or chaperone-mediated activities interact with the DPD→AI-2 reaction or other pathways lead to a substantial (~2 to 3-fold) increase in flux to DPD within the cell. Hauck *et al* (2003) already demonstrated the existence of an alternative pathway to AI-2 and Tavender *et al* (2004) showed that ribulose-5-phosphate can strongly induce the bioluminescence of AI-2-specific response reporter). Adenosine can be shunted to ribulose-5-phosphate through pentose phosphate metabolism; therefore, we suspect that ribose sugar phosphates may be possible candidates for conversion to AI-2. Independently, we measured transcript levels of the enzymes involved in the oxidative pentose phosphate pathway (catalyzing reactions from glucose-6-phosphate to ribulose-5-phosphate) and they were observed to increase about 1.4- to 2.1-fold owing to the presence of glucose (in DNA microarray experiments not shown here; Wang *et al*, in preparation). Increased activity of these enzymes may yield more ribulose-5-phosphate, a putative precursor for AI-2 (Hauck *et al*, 2003; Tavender *et al*, 2004).

It is particularly noteworthy that there are two different structures of AI-2 reported from the same precursor, DPD (Chen *et al*, 2002; Miller *et al*, 2004), in two different biological systems. If there is more than one reaction for producing or consuming one metabolite, it is more likely that one reaction dominates (Almaas *et al*, 2004). Based on this theory, one autoinducer structure should be favored. Bassler and co-workers (Miller *et al*, 2004)have already demonstrated this by showing that the AI-2 structure in *V. harveyi* is distinct from that in *S. typhimurium*, where boric acid can shift the direction/equilibrium of these two different structure signal molecules. It is not unreasonable to suggest that under different biological contexts (microbe, microenvironment, etc.), the pathways for the formation of AI-2 are different. This is corroborated by our calculations demonstrating that the AI-2 synthesis rates in the absence and presence of glucose

are different and change over time. One might even expect that the resultant AI-2 structure varies as growth condition changes. Analogously, we have already demonstrated that genes affected by *luxS* mutation vary with growth condition, such as cell density or glucose addition (Wang *et al*, 2005b).

Questions such as these arise, and can be put into an experimental context, upon the examination of model simulations relative to experimental observations. The use of SPN in Mobius environment makes the implementation of a model easier than using other programming languages; there is no need to write specific code for each model. This makes it easy to replicate, modify, or extend a particular model (Goss and Peccoud, 1998), so that a large system can be decomposed into several small systems, which can then be reconstituted into more complex systems of larger scale. Indeed, our current model was originally comprised of an AI-2 synthesis model only. This makes it possible to achieve an integrated understanding of the hierarchical nature of quorum signaling regulatory cascades. For different layers of genetic pathways, from available biological information, we can construct models as we did in this study, then modify and integrate them for a global model based on experimental validation.

Materials and methods

Plasmid, bacterial strains, and culture conditions

pTrcHisC (Invitrogen) was used for construction of pTrcHis-pfs and pTrcHis-luxS. Detailed methods for plasmid construction are outlined elsewhere (Hashimoto *et al*, in preparation). These plasmids were subsequently transformed into the strains DH5α and NC13: DH5α carrying pTrcHis-pfs and NC13 carrying pTrcHis-luxS, for overexpressing Pfs and LuxS, respectively. Glucose, biotin (Cadieux *et al*, 2002), and IPTG, when present, were added at 0.8%, 10 ng/ml, and 1 mM, respectively. Bacterial strains and plasmids used in this paper are summarized in Table VI.

AI-2 activity assay

E. coli cell-free culture supernatants were tested for the presence of AI-2 using the *V. harveyi* reporter strain BB170 (Surette and Bassler, 1998). Briefly, 20 μl of AI-2 cell-free supernatant was mixed with 180 μl of BB170 suspension, which was prepared by 5000-fold dilution of a 16-h overnight culture in AB medium. A 20 μl portion of growth medium (AB and LB medium) was added to 180 μl BB170 suspension as negative control. All the cultures were grown at 30°C and 225 r.p.m. (New Brunswick Scientific); bioluminescence was measured hourly. Fold activation was calculated by bioluminescence from experimental samples divided by that of the negative controls, and then normalized by cell optical density.

RNA preparation and Northern blot analysis

Overnight cultures grown in LB were diluted 100-fold into fresh LB and grown to mid-exponential phase, then diluted again into LB or LB with glucose at OD_{600} near 0.03. Cultures were then incubated at 30°C with shaking at 250 r.p.m. Total RNA was isolated and diluted on an OD equivalent basis from culture volumes equivalent to 1 ml at an OD_{600} of 1.0 using a Qiagen RNeasy mini kit (Qiagen, Valencia, CA). Same amount of RNA was loaded on a 1% formaldehyde agarose gel and then transferred to a positively charged nylon membrane. A digoxygenin DNA labeling and detection kit (Boehringer Mannheim) was used for labeling DNA probes and detection according to the manufacturer's instructions. For probe construction, the following oligonucleotides were used: *luxS1*
5′-CTAGATGTGCAGTTCCTGCAA-3′ and *luxS2*
5′-ATGCCGTTAGATAGCTTC-3′ for a *luxS*-specific probe; *pfs1*
5′-AATCGGGCTTATCGCGAGTAAA-3′ and *pfs2*
5′-GCAAGTTTCTGCACCAGTGACTC-3′ for a *pfs*-specific probe; *speD1*
5′-GCGCGACGGTTATATTATATC-3′ and *speD2*
5′-CGCTAATCAATGGTTACGATATCGGA-3′ for a *speD*-specific probe.
Northern results were repeated in triplicate and quantified using NIH ImageJ software.

Real-time RT–PCR

cDNA was synthesized from total RNA with random hexamers using the SuperScript™ III First-Strand Synthesis System for RT–PCR (Invitrogen) according to the manufacturer's instructions. Primers were designed and purchased from Integrated DNA Technologies (Coralville, IA). Regular PCR was used to check the uniqueness of the

Table VI Bacterial strains and plasmids used in this study

Strain/plasmid	Relevant genotype and property	Source or reference
Strains		
E. coli W3110	Wild type	Laboratory stock
E. coli LW3	ZK126 Δ*luxS*::Kan^r	Laboratory stock
E. coli MDAI2	W3110 Δ*luxS*::Tc^r	Laboratory stock
E. coli NC13	RK4353 Δ*pfs (8-226)*::Kan^r	Cadieux *et al*, 2002
E. coli DH5α	*recA1 supE44 endA1 hsdR17 gyrA96 relA1 thi*Δ *(lac-proAB)* F′ [*traD36 proAB+ lacI^q lacZ*Δ*M15*]	Invitrogen
E. coli LW2	ZK126 Δ*crp*::Kan	Wang *et al*, 2005a
V. harveyi BB152	BB120 *luxL*::Tn5 (AI-1$^-$, AI-2$^+$)	Surette and Bassler, 1998
V. harveyi BB170	BB120 *luxN*::Tn5 (sensor 1$^-$, sensor 2$^+$)	Bassler *et al*, 1993
Plasmids		
pFZY1	*galk′-lacZYA* transcriptional fusion vector, Ap^r	Koop *et al*, 1987
pLW10	pFZY1 derivative, containing *luxS* promoter, Ap^r	Wang *et al*, 2005a
pYH10	pFZY1 derivative, containing *pfs* promoter, Ap^r	Wang *et al*, 2005a
pHA7E	pBR322 derivative, *crp*$^+$ Ap^r	Joung *et al*, 1995
pIT302	pACYC184 derivative, *cya*$^+$ Cm^r	Kimata *et al*, 1997
pTrcHis C	Cloning vector, Ap^r	Invitrogen
pTrcHis-luxS	pTrcHis C derivative, *luxS*$^+$ Ap^r	Hashimoto *et al*, in preparation
pTrcHis-pfs	pTrcHis C derivative, *pfs*$^+$ Ap^r	Hashimoto *et al*, in preparation

Table VII Primers used in real-time PCR

Gene	Direction	Primer sequence
16S rRNA	Upstream	5′-CAGCCACACTGGAACTGAGA-3′
	Downstream	5′-GTTAGCCGGTGCTTCTTCTG-3′
luxS	Upstream	5′-CATACCCTGGAGCACCTGTT-3′
	Downstream	5′-TGATCCTGCACTTTCAGCAC-3′
pfs	Upstream	5′-GAGGTTGCGCTTCTGAAATC-3′
	Downstream	5′-GACAACGATATCGCCCACTT-3′

primers before using the cDNA for quantification PCR. Real-time RT–PCR was performed in 50 μl of reaction mixture containing the Platinum SYBR Green qPCR Supermix UDG (Invitrogen), 0.2 μM of primers, and cDNA (50°C, 2 min; 95°C, 2 min; 95°C, 15 s, 40 cycles; 60°C, 1 min). The reaction and detection of dye-labeled PCR products were performed with an Applied Biosystems 7300 Real-time PCR System (Applied Biosystems). *16S rRNA* was used as the endogenous control and primers are listed in Table VII. Samples obtained from the 3 h time points of the LB with 0.8% glucose cultures were used to normalize data.

SDS–PAGE analysis

Culture volumes equivalent to 2 ml at an OD_{600} of 1.0 were withdrawn at the growth of 6 h time point and spun down at 12 000 r.p.m. for 5 min in a microcentrifuge. The cell pellets were resuspended and lysed in 300 μl BugBuster protein extraction reagent (Novagen) under room temperature for 30 min and then spun down at 12 000 r.p.m. for 10 min. The soluble cell extract was 1:1 (v/v) mixed with sodium dodecyl sulfate (SDS) sampling buffer (12.5% 0.5 M Tris–HCl (pH 6.8), 10% glycerol, 2% SDS, 5% β-mercaptoethanol, 0.0025% bromophenol blue), heated at 100°C for 5 min, and vortexed. Samples were loaded onto a 15% SDS–polyacrylamide gel for electrophoresis. Proteins were visualized by staining with Coomassie blue and quantified after developing linearized standard curves with purified proteins.

Supplementary information

Supplementary information is available at the *Molecular Systems Biology* website (www.nature.com/msb).

Acknowledgements

We thank BL Bassler, H Aiba, R Kolter, A Hochschild, LI Rothfield, and M Berlyn for generously providing strains and plasmids used in the study. We are very grateful to Daniel Mitchell and Stephen Ramsey for the wonderful discussions and suggestions about SBML. We are grateful J March for the proofreading. This work was supported by the National Science Foundation (grants BES-0124401 and BES-0222687).

References

Almaas E, Kovacs B, Vicsek T, Oltvai ZN, Barabasi A (2004) Global organization of metabolic fluxes in the bacterium *Escherichia coli*. *Nature* **427:** 839–843

Arkin A, Ross J, McAdams HH (1998) Stochastic kinetic analysis of developmental pathway bifurcation in phage lambda-infected *Escherichia coli* cells. *Genetics* **149:** 1633–1648

Balestrino D, Haagensen JA, Rich C, Forestier C (2005) Characterization of type 2 quorum sensing in *Klebsiella pneumoniae* and relationship with biofilm formation. *J Bacteriol* **187:** 2870–2880

Bassler BL, Wright M, Showalter RE, Silverman MR (1993) Intercellular signalling in *Vibrio harveyi*: sequence and function of genes regulating expression of luminescence. *Mol Microbiol* **9:** 773–786

Bassler BL, Wright M, Silverman MR (1994) Multiple signalling systems controlling expression of luminescence in *Vibrio harveyi*: sequence and function of genes encoding a second sensory pathway. *Mol Microbiol* **13:** 273–286

Bowman WH, Tabor CW, Tabor H (1973) Spermidine biosynthesis. Purification and properties of propylamine transferase from *Escherichia coli*. *J Biol Chem* **248:** 2480–2486

Bremer H, Dennis P (1996) Modulation of chemical composition and other parameters of the cell by growth rate. In *Escherichia coli and Salmonella: Cellular and Molecular Biology*, Neidhardt F (ed) Vol. 2, pp 1553–1569. Washington, DC: ASM Press

Cadieux N, Bradbeer C, Reeger-Schneider E, Koster W, Mohanty AK, Wiener MC, Kadner RJ (2002) Identification of the periplasmic cobalamin-binding protein BtuF of *Escherichia coli*. *J Bacteriol* **184:** 706–717

Chen X, Schauder S, Potier N, Van Dorsselaer A, Pelczer I, Bassler BL, Hughson FM (2002) Structural identification of a bacterial quorum-sensing signal containing boron. *Nature* **415:** 545–549

Cohen S (1998) *A Guide to the Polyamines*. New York: Oxford University Press

De Keersmaecker SC, Varszegi C, van Boxel N, Habel LW, Metzger K, Daniels R, Marchal K, De Vos D, Vanderleyden J (2005) Chemical synthesis of (*S*)-4,5-dihydroxy-2,3-pentanedione, a bacterial signal molecule precursor, and validation of its activity in *Salmonella typhimurium*. *J Biol Chem* **280:** 19563–19568

Della Ragione F, Porcelli M, Cartenì-Farina M, Zappia VaP, Pegg AE (1985) *Escherichia coli S*-adenosylhomocysteine/5′-methylthio-adenosine nucleosidase. Purification, substrate specificity and mechanism of action. *Biochem J* **232:** 335–341

DeLisa MP, Valdes JJ, Bentley WE (2001a) Mapping stress-induced changes in autoinducer AI-2 production in chemostat-cultivated *Escherichia coli* K-12. *J Bacteriol* **183:** 2918–2928

DeLisa MP, Valdes JJ, Bentley WE (2001b) Quorum signaling via AI-2 communicates the 'Metabolic Burden' associated with heterologous protein production in *Escherichia coli*. *Biotechnol Bioeng* **75:** 439–450

Draper D (1996) Tranlational initiation. In *Escherichia coli and Salmonella*, Neidhardt FC (ed) Vol. 1, pp 902–921. Washington, DC: ASM Press

Duerre J (1962) A hydrolytic nucleosidase acting on *S*-adenosylhomocysteine and on 5′-methylthioadenosine. *J Biol Chem* **237:** 3737–3741

Federle MJ, Bassler BL (2003) Interspecies communication in bacteria. *J Clin Invest* **112:** 1291–1299

Fuqua C, Greenberg EP (1998) Self perception in bacteria: quorum sensing with acylated homoserine lactones. *Curr Opin Microbiol* **1:** 183–189

Fuqua C, Parsek MR, Greenberg EP (2001) Regulation of gene expression by cell-to-cell communication: acyl-homoserine lactone quorum sensing. *Annu Rev Genet* **35:** 439–468

Gibson MA, Mjolsness E (2001) Modeling of the activity of single genes. In *Computational Modeling of Genetic and Biochemical Networks*, Bolouri, JMBaH (ed) pp 1–48. Cambrige: MIT Press

Gillespie DT (1977) Exact stochastic simulation of coupled chemical reactions. *J Phys Chem* **81:** 2340–2361

Goss PJ, Peccoud J (1998) Quantitative modeling of stochastic systems in molecular biology by using stochastic Petri nets. *Proc Natl Acad Sci USA* **95:** 6750–6755

Hamada K, Ago H, Sugahara M, Nodake Y, Kuramitsu S, Miyano M (2003) Oxyanion hole-stabilized stereospecific isomerization in ribose-5-phosphate isomerase (Rpi). *J Biol Chem* **278:** 49183–49190

Hauck T, Hubner Y, Bruhlmann F, Schwab W (2003) Alternative pathway for the formation of 4,5-dihydroxy-2,3-pentanedione, the proposed precursor of 4-hydroxy-5-methyl-3(2*H*)-furanone as well as autoinducer-2, and its detection as natural constituent of tomato fruit. *Biochim Biophys Acta* **1623:** 109–119

Hofmann T (1998) Characterization of the chemical structure of novel colored Maillard reaction products from furan-2-carboxaldehyde and amino acids. *J Agric Food Chem* **46:** 932–940

Holms H (1996) Flux analysis and control of the central metabolic pathways in *E. coli*. *FEMS Microbiol Rev* **19:** 85–116

Ingraham J, Maaloe O, Neidhardt F (1983) *Growth of the Bacterial Cell*. Sunderland, MA: Sinaeur Associates Inc.

Isbell HS, Pigman W (1969) Mutarotation of sugars in solutions: II. Catalytic processes, isotope effects, reaction mechanisms, and biochemical aspects. *Adv Carbohydrate Chem Biochem* **24:** 13–65

Joung JK, Chung EH, King G, Yu C, Hirsh AS, Hochschild A (1995) Genetic strategy for analyzing specificity of dimer formation: *Escherichia coli* cyclic AMP receptor protein mutant altered in its dimerization specificity. *Genes Dev* **9:** 2986–2996

Kashiwagi K, Pistocchi R, Shibuya S, Sugiyama S, Morikawa K, Igarashi K (1996) Spermidine-preferential uptake system in *Escherichia coli*. Identification of amino acids involved in polyamine binding in PotD protein. *J Biol Chem* **271:** 12205–12208

Kimata K, Takahashi H, Inada T, Postma P, Aiba H (1997) cAMP receptor protein-cAMP plays a crucial role in glucose-lactose diauxie by activating the major glucose transporter gene in *Escherichia coli*. *Proc Natl Acad Sci USA* **94:** 12914–12919

Koop AH, Hartley ME, Bourgeois S (1987) A low-copy-number vector utilizing beta-galactosidase for the analysis of gene control elements. *Gene* **52:** 245–256

Kushner S (1996) mRNA decay. In *Escherichia coli and Salmonella*, Neidhardt FC (ed) Vol. 1, pp 849–860. Washington, DC: SAM Press

Li J, Wang L, Zafiriou E, Bentley WE (2004) Investigation of transport and uptake of autoinducer-2 (AI-2) in *Escherichia coli*. In *AICHE Annual Meeting*. Houston, TX

Matsuno H, Doi A, Nagasaki M, Miyano S (2000) *Hybrid Petri Nets Representation of Gene Regulatory Network*. Singapore: World Scientific Publishing

McAdams HH, Arkin A (1997) Stochastic mechanism in gene expression. *Proc of Natl Acad Sci USA* **94:** 814–819

McAdams HH, Arkin A (1999) It's a noisy business! genetic regulation at the nanomolar scale. *Trends Genet* **15:** 65–69

Meijler MM, Hom LG, Kaufmann GF, McKenzie KM, Sun C, Moss JA, Matsushita M, Janda KD (2004) Synthesis and biological validation of a ubiquitous quorum-sensing molecule. *Angew Chem Int Ed Engl* **43:** 2106–2108

Mettetal JT, Muzzey D, Pedraza JM, Ozbudak EM, van Oudenaarden A (2006) Predicting stochastic gene expression dynamics in single cells. *Proc Natl Acad Sci USA* **103:** 7304–7309

Miller MB, Bassler BL (2001) Quorum sensing in bacteria. *Annu Rev Microbiol* **55:** 165–199

Miller ST, Xavier KB, Campagna SR, Taga ME, Semmelhack MF, Bassler BL, Hughson FM (2004) *Salmonella typhimurium* recognizes a chemically distinct form of the bacterial quorum-sensing signal AI-2. *Mol Cell* **15:** 677–687

Nealson KH, Platt T, Hastings JW (1970) Cellular control of the synthesis and activity of the bacterial luminescence system. *J Bacteriol* **104:** 313–322

Neidhardt F, Ingraham J, Schaechter M (1990) *Physiology of the Bacterial Cell: A Molecular Approach*, pp 8–9. Sunderland, Mass: Sinauer Associates Inc

Newman EB, Budman LI, Chan EC, Greene RC, Lin RT, Woldringh CL, D'Ari R (1998) Lack of *S*-adenosylmethionine results in a cell division defect in *Escherichia coli*. *J Bacteriol* **180:** 3614–3619

Oh MK, Liao JC (2000) Gene expression profiling by DNA microarrays and metabolic fluxes in *Escherichia coli*. *Biotechnol Prog* **16:** 278–286

Pedersen S, Bloch P, Reeh S, Neidhardt F (1978) Patterns of protein synthesis in *E. coli*: a catalog of the amount of 140 individual proteins at different growth rates. *Cell* **14:** 179–190

Pigman W, Isbell HS (1968) Mutarotation of sugars in solution: I. history, basic kinetics, and composition of sugar solutions. *Adv Carbohydrate Chem* **23:** 11–57

Posnick LM, Samson LD (1999) Influence of *S*-adenosylmethionine pool size on spontaneous mutation, dam methylation, and cell growth of *Escherichia coli*. *J Bacteriol* **181:** 6756–6762

Records Jr MT, Reznikoff WS, Craig ML, McQuade KL, Schlax PJ (1996) *Escherichia coli* RNA polymerase(Esigma70), promoters, and the kinetics of the steps of transcription initiation. In *Escherichia coli and Salmonella*, Neidhardt FC (ed) Vol. 1, pp 792–820. Washington, DC: ASM Press

Roe AJ, O'Byrne C, McLaggan D, Booth IR (2002) Inhibition of *Escherichia coli* growth by acetic acid: a problem with methionine biosynthesis and homocysteine toxicity. *Microbiology* **148:** 2215–2222

Schauder S, Shokat K, Surette MG, Bassler BL (2001) The LuxS family of bacterial autoinducers: biosynthesis of a novel quorum-sensing signal molecule. *Mol Microbiol* **41:** 463–476

Schroeder HR, Barnes CJ, Bohinski RC, Mallette MF (1973) Biological production of 5-methylthioribose. *Can J Microbiol* **19:** 1347–1354

Semmelhack MF, Campagna SR, Hwa C, Federle MJ, Bassler BL (2004) Boron binding with the quorum sensing signal AI-2 and analogues. *Org Lett* **6:** 2635–2637

Semmelhack MF, Campagna SR, Federle MJ, Bassler BL (2005) An expeditious synthesis of DPD and boron binding studies. *Org Lett* **7:** 569–572

Simms SA, Stock AM, Stock JB (1987) Purification and characterization of the *S*-adenosylmethionine:glutamyl methyltransferase that modifies membrane chemoreceptor proteins in bacteria. *J Biol Chem* **262:** 8537–8543

Smolen P, Baxter DA, Byrne JH (2000) Mathematical modeling of gene networks. *Neuron* **26:** 567–580

Sorensen KI, Hove-Jensen B (1996) Ribose catabolism of *Escherichia coli*: characterization of the rpiB gene encoding ribose phosphate isomerase B and of the rpiR gene, which is involved in regulation of rpiB expression. *J Bacteriol* **178:** 1003–1011

Sperandio V, Torres AG, Jarvis B, Nataro JP, Kaper JB (2003) Bacteria-host communication: the language of hormones. *Proc Natl Acad Sci USA* **100:** 8951–8956

Sperandio V, Torres AG, Kaper JB (2002) Quorum sensing *Escherichia coli* regulators B and C (QseBC): a novel two-component regulatory system involved in the regulation of flagella and motility by quorum sensing in *E. coli*. *Mol Microbiol* **43:** 809–821

Srivastava R, Peterson MS, Bentley WE (2001) Stochastic kinetic analysis of the *Escherichia coli* stress circuit using sigma(32)-targeted antisense. *Biotechnol Bioeng* **75:** 120–129

Sturme MH, Kleerebezem M, Nakayama J, Akkermans AD, Vaugha EE, de Vos WM (2002) Cell to cell communication by autoinducing peptides in Gram-positive bacteria. *Antonie van Leeuwenhoek* **81:** 233–243

Surette MG, Bassler BL (1998) Quorum sensing in *Escherichia coli* and *Salmonella typhimurium*. *Proc Natl Acad Sci USA* **95:** 7046–7050

Surette MG, Miller MB, Bassler BL (1999) Quorum sensing in *Escherichia coli*, *Salmonella typhimurium*, and *Vibrio harveyi*: a new family of genes responsible for autoinducer production. *Proc Natl Acad Sci USA* **96:** 1639–1644

Taga ME, Miller ST, Bassler BL (2003) Lsr-mediated transport and processing of AI-2 in *Salmonella typhimurium*. *Mol Microbiol* **50:** 1411–1427

Tavender T, Baldwin TJ, Hardie KR, Winzer K (2004) LuxS independent AI-2 production:proposal of a novel non-enzymatic route. In *ASM 2004 General Meeting*

Taylor JC, Takusagawa F, Markham GD (2002) The active site loop of *S*-adenosylmethionine synthetase modulates catalytic efficiency. *Biochemistry* **41:** 9358–9369

Vendeville A, Winzer K, Heurlier K, Tang CM, Hardie KR (2005) Making 'sense' of metabolism: autoinducer-2, LuxS and pathogenic bacteria. *Nat Rev Microbiol* **3:** 383–396

Wang L, Hashimato Y, Tsao C, Valdes JJ, Bentley WE (2005a) cAMP and cAMP receptor (CRP) influence both synthesis and uptake of extracellular autoinducer-2 in *E. coli*. *J Bacteriol* **187:** 2066–2076

Wang L, Li J, March JC, Valdes JJ, Bentley WE (2005b) *luxS*-dependent gene regulation in *Escherichia coli* K-12 revealed by genomic expression profiling. *J Bacteriol* **187:** 8350–8360

Westerhoff HV, Palsson BO (2004) The evolution of molecular biology into systems biology. *Nat Biotechnol* **22:** 1249–1252

Wickner RB, Tabor CW, Tabor H (1970) Purification of adenosylmethionine decarboxylase from *Escherichia coli* W: evidence for covalently bound pyruvate. *J Biol Chem* **245:** 2132–2139

Williams SC, Patterson EK, Carty NL, Griswold JA, Hamood AN, Rumbaugh KP (2004) *Pseudomonas aeruginosa* autoinducer enters and functions in mammalian cells. *J Bacteriol* **186:** 2281–2287

Winzer K, Hardie KR, Burgess N, Doherty N, Kirke D, Holden MT, Linforth R, Cornell KA, Taylor AJ, Hill PJ, Williams P (2002) LuxS: its role in central metabolism and the *in vitro* synthesis of 4-hydroxy-5-methyl-3(2*H*)-furanone. *Microbiology* **148:** 909–922

Winzer K, Hardie KR, Williams P (2003) LuxS and autoinducer-2: their contribution to quorum sensing and metabolism in bacteria. *Adv Appl Microbiol* **53:** 291–396

Withers H, Swift S, Williams P (2001) Quorum sensing as an integral component of gene regulatory networks in Gram-negative bacteria. *Curr Opin Microbiol* **4:** 186–193

Xavier KB, Bassler BL (2003) LuxS quorum sensing: more than just a numbers game. *Curr Opin Microbiol* **6:** 191–197

Xavier KB, Bassler BL (2005) Regulation of uptake and processing of the quorum-sensing autoinducer AI-2 in *Escherichia coli*. *J Bacteriol* **187:** 238–248

Xie QW, Tabor CW, Tabor H (1989) Spermidine biosynthesis in Escherichia coli: promoter and termination regions of the speED operon. *J Bacteriol* **171:** 4457–4465

Yi X, Weis RM (2002) The receptor docking segment and *S*-adenosyl-L-homocysteine bind independently to the methyltransferase of bacterial chemotaxis. *Biochim Biophys Acta* **1596:** 28–35

Yoshida A, Ansai T, Takehara T, Kuramitsu HK (2005) LuxS-based signaling affects *Streptococcus* mutants biofilm formation. *Appl Environ Microbiol* **71:** 2372–2380

Zhu J, Miller MB, Vance RE, Dziejman M, Bassler BL, Mekalanos JJ (2002) Quorum-sensing regulators control virulence gene expression in *Vibrio cholerae*. *Proc Natl Acad Sci USA* **99:** 3129–3134

Zhu J, Dizin E, Hu X, Wavreille A, Park JaP, Pei D (2003) *S*-ribosylhomocysteinase (LuxS) is a mononuclear iron protein. *Biochemistry* **42:** 4717–4726